

# Unconditionally stable, second-order accurate schemes for solid state phase transformations driven by mechano-chemical spinodal decomposition

K. Sagiya<sup>\*</sup>, S. Rudraraju<sup>†</sup> & K. Garikipati<sup>‡</sup>

June 21, 2022

## Abstract

We consider solid state phase transformations that are caused by free energy densities with domains of non-convexity in strain-composition space. We refer to the non-convex domains as mechano-chemical spinodals. The non-convexity with respect to composition causes segregation into phases with different crystal structures. If, for one of these crystal structures, the free energy density is also non-convex with respect to strain, there is potential for the corresponding phase to further separate into multiple variants. For mathematical well-posedness, and physically meaningful solutions, the free energy description must be enhanced by interface terms that penalize gradients with respect to strain and composition. A system of partial differential equations results that couples the classical Cahn-Hilliard equation with those of gradient elasticity. Since the materials systems of interest display finite strains, the appropriate description is Toupin's theory of gradient elasticity at finite strains. The presence of strain and composition gradients in the free energy density leads to fourth-order partial differential equations in primal form, and requires greater continuity of basis functions, which we satisfy by adopting splines in the setting of isogeometric analysis. This mechano-chemically coupled system of equations encompasses several simpler cases of phase transformations, and can be extended to others. Here, we develop a class of integration algorithms for time-dependent problems of phase transformations that are governed by the coupling of the Cahn-Hilliard and Toupin-gradient elasticity equations. Our goals are unconditional stability and second-order accuracy in time, motivated by the need to carry out large scale computations of dynamically evolving microstructures in three dimensions and for general initial/boundary value problems. Apart from an analysis and construction of methods that satisfy these requirements, we present a suite of numerical results that demonstrate the schemes in action.

## 1 Introduction

Many multi-component solids undergo phase-transformations in which a diffusional redistribution of their different components is coupled with a structural change of the crystallographic unit cell. One example is the phase-transformation of yttria-stabilized zirconia  $Zr_{1-x}Y_xO_{2-x/2}$  from cubic at high-Y composition to tetragonal at low-Y if quenched to a low temperature. Another is observed in the spinel structures of Li-ion electrodes when cubic  $LiMnO_4$  transforms into tetragonal  $Li_2Mn_2O_4$  upon discharging to low voltages. Pure  $ZrO_2$  and  $TaS_2$  are other materials that may be susceptible to such mechano-chemical phase transformations.

The phenomenology underlying this phenomenon can be traced to the free energy density function, which is non-convex in its mechanical (strain) and chemical (composition) arguments. Cahn and Hilliard [2] famously introduced the chemical spinodal as the domain in composition space where the free energy density is non-convex, and varies smoothly between local minima that correspond to distinct phases. This notion has recently been extended to the mechano-chemical spinodal, defined as the domain in strain-composition space where the Hessian of the (sufficiently smooth) free energy density function has non-positive eigenvalues [8]. If the state of a material point lies within the mechano-chemical spinodal, and specifically if the free energy density is non-convex with respect to composition, the solid will undergo diffusional segregation. Here we concern ourselves with cases in which the two resulting phases have cubic and tetragonal crystal structures, respectively. Importantly, the distortion of the cubic into the tetragonal lattice is naturally described by the strain relative to the cubic structure as a reference. The symmetries of the cubic lattice split into three identical sub-groups, each

<sup>\*</sup>Department of Mechanical Engineering, University of Michigan

<sup>†</sup>Department of Mechanical Engineering, University of Michigan

<sup>‡</sup>Departments of Mechanical Engineering, and Mathematics, University of Michigan, corresponding author, [krishna@umich.edu](mailto:krishna@umich.edu)

of which corresponds to a tetragonal lattice oriented along one of the cubic crystal axes. These three tetragonal variants, however, correspond to different strains relative to the reference cubic lattice. The free energy density function admits three additional minima, each corresponding to the strain that transforms the reference cubic lattice into one of the tetragonal variants. As the states of material points traverse such a multi-welled free energy density surface in strain-composition space the solid develops a microstructure. The mechano-chemical spinodal is regarded as a domain of instability since small fluctuations in strain and composition tend to grow as the state evolves towards one of the wells in strain-composition space. Stress softening and “uphill” diffusion result, respectively.

A non-convex free energy density function can lead to microstructure as explained above. However, a mathematical model restricted to the above phenomenology leads to ill-posed partial differential equations (PDEs) for elasticity and transport characterized by spurious mesh dependence. The volume fractions of the cubic and tetragonal phases would be set by initial and boundary conditions on the transport problem, and the volume fractions of the tetragonal variants would depend on mechanical boundary conditions. However, in the absence of an intrinsic length scale in the mathematical model, this size would be determined by the mesh. There is a well-understood physical aspect to this argument, also: The model promotes free energy minimizing microstructures, but incurs no penalty for the rapidity with which strain and composition fields fluctuate between one phase or variant and the next. Arbitrarily fine energy minimizing microstructures are therefore admissible—an essentially unphysical result. Mathematical well-posedness and physical realism are restored by extending the free energy density function to include a dependence on gradient fields of strain and composition. The corresponding free energy coefficients introduce intrinsic length scales, and the gradient energies distinguish between microstructures of differing fineness, penalizing those that vary rapidly.

Gradient free energies in classical settings lead to the Cahn-Hilliard equation for mass transport [2], and variants of strain gradient elasticity that represent size effects. Because the transformation strains between the cubic/tetragonal phases and between the tetragonal variants are of finite magnitude in many material systems, we are led to Toupin’s theory of nonlinear (finite strain) gradient elasticity [9]. The Cahn-Hilliard equation and Toupin’s strain gradient elasticity present fourth-order spatial derivatives in primal strong form. The corresponding weak forms have second-order derivatives, implying a  $C^1$ -continuity (up to first spatial derivatives). They thus present challenges to standard finite element implementations whose finite dimensional function spaces are built upon  $C^0$ -continuous Lagrange polynomials.

Gómez and co-workers [4] employed isogeometric analysis (IGA), exploiting its ease of constructing basis functions with arbitrary order of continuity, to solve the Cahn-Hilliard equation in three dimensions. Their time integration scheme used the generalized- $\alpha$  method, embedded Runge-Kutta schemes and an adaptive time step selection criterion. Rudraraju and co-workers also used IGA to present the first solutions to Toupin’s theory of gradient elasticity at finite strains [7]. More recently the same authors have combined IGA for spatial discretization with the Backward Euler algorithm [8] to solve the same problem that we consider here. However, in that work the authors concerned themselves with introducing the notion of the mechano-chemical spinodal, and exploring the associated physics; not with an analysis of the algorithms which is the goal of the present communication. Gómez & Hughes, however, adopted a more classical approach for the Cahn-Hilliard equation by decomposing it into two second-order PDEs [5], one of which relates the chemical potential to the sum of a so-called homogeneous term and the Laplacian of the composition. This split formulation presents only up to second-order spatial derivatives in strong form, and first-order derivatives in weak form. Therefore  $C^0$ -continuous function spaces are admissible. In particular, standard mixed finite element methods can be applied. Dedicated quadrature formula were then applied to the chemical free energy, producing the expression for the time-discrete chemical potential that renders their formulation unconditionally stable and second-order accurate. Numerical examples were shown in two dimensions. Unconditionally stable second-order accurate time-integration schemes were also proposed by Vignal and co-workers [10] for the sixth-order phase-field crystal equation, and by Han & Wang [6] for the Cahn-Hilliard-Navier-Stokes system of equations. Both formulations were inspired by the split formulation of the Cahn-Hilliard equation and employed the idea of *convex splitting*; the chemical free energy was split into convex and concave parts, the former treated implicitly and the latter explicitly.

For the coupled system of the Cahn-Hilliard phase-field model and Toupin’s strain gradient elasticity at finite strains that we consider in this work, the split formulation is used for the transport problem as in [5], while the higher-order spatial derivatives existing in the gradient equations are directly treated by IGA as in [7]. We then develop a novel time-integration algorithm for the resulting spatially discrete formulation that is proven to be second-order accurate and unconditionally stable. Our stability analysis draws partly from the work of Gómez & Hughes [5] for the Cahn-Hilliard equation; however, we use a multi-variate Taylor series expansion instead of dedicated quadrature formula, which allows for a consistent treatment of the coupling with strain gradient elasticity. To our knowledge this is the first unconditionally stable time-integration algorithm for mechano-chemical phase-transformation problems. Of note is the incorporation of gradient elasticity at finite strains—a feature that adds considerable complexity to the equations.

In Sec.2 we present the variational formulation of our mechano-chemical problem. The corresponding spatially and temporally discrete formulations are developed in Sec.3. Unconditional stability and second-order

accuracy of our fully discrete formulation are studied in Sec.4. Finally, a suite of numerical examples is presented in Sec.5 to demonstrate the performance of the algorithms in three dimensions. Final remarks are made and future work proposed in Sec.6.

## 2 Variational formulations for the coupled mechano-chemical spinodal decomposition

We consider the mechano-chemical spinodal decomposition in a body that occupies at the reference time a bounded domain  $\Omega$  in three-dimensional Euclidean space in which we introduce the rectangular Cartesian coordinate system with  $X_J$  ( $J = 1, 2, 3$ ) the corresponding coordinate variables.

We are interested in the chemical concentration field  $c(\mathbf{X}, t)$  and the mechanical displacement field  $\mathbf{u}(\mathbf{X}, t)$  in  $\Omega$ . In this section we assume that these quantities and their spatial derivatives are continuously defined in the neighborhood of  $\bar{\Omega}$ . The boundary of  $\Omega$  is assumed to be decomposed into a finite number of smooth surfaces  $\Gamma_\iota$ , smooth curves  $\Upsilon_\iota$ , and points  $\Xi_\iota$ , so that  $\partial\Omega = \Gamma \cup \Upsilon \cup \Xi$  where  $\Gamma = \cup_\iota \Gamma_\iota$ ,  $\Upsilon = \cup_\iota \Upsilon_\iota$ , and  $\Xi = \cup_\iota \Xi_\iota$ . Each surface  $\Gamma_\iota$  and curve  $\Upsilon_\iota$  is further divided into mutually exclusive Dirichlet and Neumann subsets that are represented, respectively, by superscripts of lowercase letters  $u$ ,  $m$ , and  $g$  and those of uppercase letters  $T$ ,  $M$ , and  $G$ , as  $\Gamma_\iota = \Gamma_\iota^u \cup \Gamma_\iota^T = \Gamma_\iota^m \cup \Gamma_\iota^M$  and  $\Upsilon_\iota = \Upsilon_\iota^g \cup \Upsilon_\iota^G$ . We also denote by  $\Gamma^u = \cup_\iota \Gamma_\iota^u$ ,  $\Gamma^T = \cup_\iota \Gamma_\iota^T$ ,  $\Gamma^m = \cup_\iota \Gamma_\iota^m$ ,  $\Gamma^M = \cup_\iota \Gamma_\iota^M$ ,  $\Gamma^g = \cup_\iota \Upsilon_\iota^g$ , and  $\Gamma^G = \cup_\iota \Upsilon_\iota^G$  the unions of the Dirichlet and Neumann boundaries. Our formulation and analysis presented in the following are to be readily extended to include mixed boundary conditions. As in [9], coordinate derivatives of a scalar function  $\phi$  are decomposed on  $\Gamma$  into normal and tangential components as:

$$\phi_{,J} = D\phi N_J + D_J\phi,$$

where

$$\begin{aligned} D\phi &:= \phi_{,K} N_K, \\ D_J\phi &:= \phi_{,J} - \phi_{,K} N_K N_J, \end{aligned}$$

where  $N_J$  are the components of the unit outward normal to  $\Gamma$ . Here as elsewhere  $(\cdot)_{,J}$  denotes the spatial derivative with respect to the reference coordinate variable  $X_J$ .

Dirichlet boundary conditions for the displacement field  $\mathbf{u}$  can now be given as:

$$u_i = \bar{u}_i \quad \text{on } \Gamma^u, \quad Du_i = \bar{m}_i \quad \text{on } \Gamma^m, \quad u_i = \bar{g}_i \quad \text{on } \Upsilon^g, \quad (1)$$

where  $\bar{u}_i$ ,  $\bar{m}_i$ , and  $\bar{g}_i$  are components of known vector functions on  $\Gamma^u$ ,  $\Gamma^m$ , and  $\Upsilon^g$ . On the other hand, we denote the components of the standard surface traction on  $\Gamma^T$ , the higher-order traction on  $\Gamma^M$ , and the line traction on  $\Upsilon^G$  by  $\bar{T}_i$ ,  $\bar{M}_i$ , and  $\bar{G}_i$ , whose mathematical formulas will be clarified in Sec.2.3. The chemical concentration field  $c$  is assumed to have no Dirichlet boundary conditions throughout  $\Gamma$ .

### 2.1 Free energy

We derive the IBVP for the mechano-chemical spinodal decomposition inspired by the variational formulation. The total free energy that we consider in this work is a functional of  $c$  and  $\mathbf{u}$  defined as:

$$\Pi[c, \mathbf{u}] := \int_{\Omega} \Psi_c + \Psi_s + \Psi_e \, dV - \int_{\Gamma^T} u_i \bar{T}_i \, dS - \int_{\Gamma^M} Du_i \bar{M}_i \, dS - \int_{\Upsilon^G} u_i \bar{G}_i \, dC, \quad (2)$$

where  $\Psi_c(c)$ ,  $\Psi_s(c, c_{,A})$ , and  $\Psi_e(c, F_{iJ}, F_{iJ,K})$  are the chemical, surface, and mechanical free energy densities that are functions of  $c$ ,  $c_{,A}$ ,  $F_{iJ}$ , and/or  $F_{iJ,K}$  at each fixed point  $\mathbf{X} \in \Omega$ , where  $F_{iJ} = \delta_{iJ} + u_{i,J}$  are the components of the deformation gradient tensor. These free-energy densities are explicitly defined as:

$$\Psi_c := A_1 (c \log c + (1 - c) \log (1 - c)) + A_2 c (1 - c), \quad (3a)$$

$$\Psi_s := \frac{1}{2} c_{,A} K_{AB}(c) c_{,B}, \quad (3b)$$

$$\begin{aligned} \Psi_e &:= B_1(c) (e_1 - e_{\text{chem}}(c))^2 \\ &\quad + B_2(c) (e_2^2 + e_3^2) + B_3(c) e_3 (e_3^2 - 3e_2^2) + B_4(c) (e_2^2 + e_3^2)^2 + B_5(c) (e_4^2 + e_5^2 + e_6^2) \\ &\quad + B_6(c) (e_{2,1}^2 + e_{2,2}^2 + e_{2,3}^2 + e_{3,1}^2 + e_{3,2}^2 + e_{3,3}^2), \end{aligned} \quad (3c)$$

where  $A_1$  and  $A_2$  are constants,  $e_{\text{chem}}(c), B_1(c), \dots, B_7(c)$  are polynomial functions of  $c$ ,  $K_{AB}(c)$  are the components of the symmetric diffusion tensor that are assumed to be polynomial functions of  $c$ , and finally  $e_1, \dots, e_6$  are symmetry strains defined as:

$$e_1 = (E_{11} + E_{22} + E_{33})/\sqrt{3}, \quad (4a)$$

$$e_2 = (E_{11} - E_{22})/\sqrt{2}, \quad (4b)$$

$$e_3 = (E_{11} + E_{22} - 2E_{33})/\sqrt{6}, \quad (4c)$$

$$e_4 = E_{23} = E_{32}, \quad (4d)$$

$$e_5 = E_{13} = E_{31}, \quad (4e)$$

$$e_6 = E_{12} = E_{21}, \quad (4f)$$

where  $E_{IJ} = 1/2(F_{kI}F_{kJ} - \delta_{IJ})$  are the components of the Lagrangian strain tensor. To facilitate formulation and analysis, we denote by  $\zeta$  an array of  $c, c_{,A}, F_{iJ},$  and  $F_{iJ,K}$  and define a new multi-variate scalar function  $\Psi_{s+e} := \Psi_s + \Psi_e$ . Note that, from definitions (3b), (3c), and (4),  $\Psi_{s+e}$  is a multi-variate polynomial function of  $c, c_{,A}, F_{iJ},$  and  $F_{iJ,K}$ , which we appreciate in developing our unconditionally stable time-integration algorithm.

## 2.2 Chemical equilibrium/non-equilibrium

In this section we derive equations for the non-equilibrium chemistry following the standard treatment. We first take the variational derivative of the total free-energy functional (2) with respect to the chemical concentration  $c$  in the direction of  $q$  to obtain:

$$\delta_c \Pi[c, \mathbf{u}] = \left. \frac{d}{d\varepsilon} \Pi[c + \varepsilon q, \mathbf{u}] \right|_{\varepsilon=0} = \int_{\Omega} q (\bar{\mu}(c) + H(\zeta)) + q_{,A} W_A(\zeta) dV, \quad (5)$$

where  $\bar{\mu}(c), H(\zeta),$  and  $W_A(\zeta)$  are defined as:

$$\bar{\mu} := \frac{d\Psi_c}{dc}, \quad (6)$$

$$H := \frac{\partial \Psi_{s+e}}{\partial c}, \quad (7)$$

$$W_A := \frac{\partial \Psi_{s+e}}{\partial c_{,A}}, \quad (8)$$

where  $\bar{\mu}(c)$  is known as the homogeneous chemical potential. At equilibrium one has  $\delta_c \Pi[c, \mathbf{u}] = 0$  and therefore from (5) one obtains the chemical-equilibrium equation as:

$$\int_{\Omega} q (\bar{\mu}(c) + H(\zeta)) + q_{,A} W_A(\zeta) dV = 0. \quad (9)$$

We then apply the divergence theorem to Eqn.(9) to obtain:

$$\int_{\Omega} q (\bar{\mu} + H - W_{A,A}) dV + \int_{\Gamma} q W_A N_A dS = 0.$$

The standard variational argument then leads us to the following strong formulation for the chemical equilibrium and the corresponding boundary condition:

$$\bar{\mu} + H - W_{A,A} = 0 \quad \text{in } \Omega, \quad (10a)$$

$$W_A N_A = 0 \quad \text{on } \Gamma. \quad (10b)$$

Note that one can further simplify Eqns.(10a) and (10b) to obtain:

$$\bar{\mu} + H - (K_{ABC,B})_{,A} = 0 \quad \text{in } \Omega,$$

$$(K_{ABC,B}) N_A = 0 \quad \text{on } \Gamma,$$

but in this work we adopt the former as it simplifies our stability analysis presented in Sec.4.2. We identify the left-hand side of Eqn.(10a) as the *chemical potential*  $\mu$ , i.e.:

$$\mu = \bar{\mu} + H - W_{A,A}. \quad (11)$$

With the expression for the chemical potential (11) in hand, one can formulate the non-equilibrium chemistry using the mass balance law in conjunction with the phenomenological representation of the flux, that is:

$$\frac{Dc}{Dt} + j_{A,A} = 0, \quad (12)$$

where

$$j_A = -L_{AB}\mu_{,B}, \quad (13)$$

where  $L_{AB}(c)$  are the components of the positive definite mobility tensor. Eqn.(12) is to require another boundary condition for  $j_A N_A$  on  $\Gamma$ . We throughout this work follow the proposition in [5] and set:

$$j_A N_A = 0 \quad \text{on } \Gamma. \quad (14)$$

In this work we adopt the mixed formulation in which  $\mu$  as well as  $c$  is regarded as a primary unknown. Multiplying Eqns.(12) and (11) by admissible test functions  $q$  and  $\nu$ , applying the divergence theorem, and applying boundary conditions (10b) and (14), one obtains the weak formulations for the chemical non-equilibrium as:

$$\int_{\Omega} q \frac{Dc}{Dt} + q_{,A} L_{AB}(c) \mu_{,B} \, dV = 0, \quad (15a)$$

$$\int_{\Omega} \nu (-\mu + \bar{\mu}(c) + H(\zeta)) + \nu_{,A} W_A(\zeta) \, dV = 0, \quad (15b)$$

where  $D/Dt$  represents the material time-derivative.

## 2.3 Mechanical equilibrium

To formulate the mechanical equilibrium, we take the variational derivative of the total free energy (2) with respect to  $\mathbf{u}$  that satisfies the Dirichlet boundary conditions (1). The test function  $\mathbf{w}$  is then to satisfy:

$$w_i = 0 \quad \text{on } \Gamma^u, \quad Dw_i = 0 \quad \text{on } \Gamma^m, \quad w_i = 0 \quad \text{on } \Upsilon^g.$$

The variational derivative is then obtained as:

$$\begin{aligned} \delta_{\mathbf{u}} \Pi[c, \mathbf{u}] &= \frac{d}{d\varepsilon} \Pi[c, \mathbf{u} + \varepsilon \mathbf{w}] \Big|_{\varepsilon=0} \\ &= \int_{\Omega} w_{i,J} P_{iJ}(\zeta) + w_{i,JK} B_{iJK}(\zeta) \, dV - \int_{\Gamma^T} w_i \bar{T}_i \, dS - \int_{\Gamma^M} Dw_i \bar{M}_i \, dS - \int_{\Upsilon^G} w_i \bar{G}_i \, dC, \end{aligned} \quad (16)$$

where  $P_{iJ}(\zeta)$  are the components of the first Piola-Kirchhoff stress tensor and  $B_{iJK}(\zeta)$  are the components of the higher-order stress tensor that are defined as:

$$\begin{aligned} P_{iJ} &:= \frac{\partial \Psi_{s+e}}{\partial F_{iJ}}, \\ B_{iJK} &:= \frac{\partial \Psi_{s+e}}{\partial F_{iJK}}. \end{aligned}$$

At equilibrium one has  $\delta_{\mathbf{u}} \Pi[c, \mathbf{u}] = 0$  so that from (16) one obtains:

$$\int_{\Omega} w_{i,J} P_{iJ}(\zeta) + w_{i,JK} B_{iJK}(\zeta) \, dV - \int_{\Gamma^T} w_i \bar{T}_i \, dS - \int_{\Gamma^M} Dw_i \bar{M}_i \, dS - \int_{\Upsilon^G} w_i \bar{G}_i \, dC = 0. \quad (17)$$

Eqn.(17) is the weak formulation for the elastic equilibrium that is to be solved in conjunction with the weak formulations for the chemical non-equilibrium (15).

The variational argument can further lead us to identify the strong formulation and the boundary conditions corresponding to (17) as the following:

$$\begin{aligned} P_{iJ,J} - B_{iJK,JK} &= 0 && \text{in } \Omega, \\ P_{iJ} N_J - B_{iJK,K} N_J - D_J (B_{iJK} N_K) + B_{iJK} (b_{LL} N_J N_K - b_{JK}) &= \bar{T}_i && \text{on } \Gamma^T, \\ B_{iJK} N_K N_J &= \bar{M}_i && \text{on } \Gamma^M, \\ \llbracket B_{iJK} N_K N_J^\Gamma \rrbracket &= \bar{G}_i && \text{on } \Upsilon^G, \end{aligned}$$

where  $b_{IJ}$  are the components of the second fundamental form on  $\Gamma^T$ ,  $N_J^\Gamma$  on  $\Upsilon_\ell \subset \Gamma_\ell^{\text{cl}}$  are the components of the unit outward normal to the surface  $\Gamma_\ell$  on a boundary  $\Upsilon_\ell$ , and  $\llbracket B_{iJK} N_K N_J^\Gamma \rrbracket$  on  $\Upsilon_\ell^G$  is the sum of  $B_{iJK} N_K N_J^\Gamma$  from two surfaces sharing  $\Upsilon_\ell^G$ ; see [9] for detail.

### 3 Numerical formulations

#### 3.1 Spatial discretization

We now discretize Eqns.(15) and (17) in space for formulations that are amenable to numerical analysis. Since  $\Psi_{s+e}$  is a function of  $F_{i,j,k}$ , our weak formulations (15) and (17) involve second-order spatial derivatives of the displacement field  $\mathbf{u}$  and the test function  $\mathbf{w}$ , which precludes application of the standard finite element methods as they only guarantee  $C^0$ -continuity on element interfaces. To overcome this difficulty, we employ the isogeometric analysis (IGA) that allows for the use of  $C^p$ -continuous basis for arbitrary order  $p$ . IGA has previously been adopted to treat higher-order spatial derivatives, e.g., in [4, 7].

We denote by  $\mathcal{S}^h$  a finite-dimensional function space spanned by a set of Non-Uniform Rational B-Splines (NURBS) basis functions that are  $C^1$ -continuous in  $\Omega$ . We then define:

$$\begin{aligned} \mathcal{V}_u^h &= \left\{ \mathbf{u}^h \in [\mathcal{S}^h]^3 : u_i^h = \bar{u}_i \quad \text{on } \Gamma^u, \quad Dw_i^h = \bar{m}_i \quad \text{on } \Gamma^m, \quad u_i^h = \bar{g}_i \quad \text{on } \Upsilon^g \right\}, \\ \mathcal{V}_w^h &= \left\{ \mathbf{w}^h \in [\mathcal{S}^h]^3 : w_i^h = 0 \quad \text{on } \Gamma^u, \quad Dw_i^h = 0 \quad \text{on } \Gamma^m, \quad w_i^h = 0 \quad \text{on } \Upsilon^g \right\}, \end{aligned}$$

assuming that this NURBS basis allows for exact representation of the Dirichlet boundary conditions (1). The proposed space-discrete counterparts of the weak formulations (15) and (17) are given as the following:

Seek  $c^h(\mathbf{X}, t) \in \mathcal{S}^h \times (0, T)$ ,  $\mu^h(\mathbf{X}, t) \in \mathcal{S}^h \times (0, T)$ ,  $\mathbf{u}^h(\mathbf{X}, t) \in \mathcal{V}_u^h \times (0, T)$  such that for all  $q^h(\mathbf{X}) \in \mathcal{S}^h$ ,  $\nu^h(\mathbf{X}) \in \mathcal{S}^h$ ,  $\mathbf{w}^h(\mathbf{X}) \in \mathcal{V}_w^h$ :

$$\int_{\Omega} q^h \frac{Dc^h}{Dt} + q_{,A}^h L_{AB}(c^h) \mu_{,B}^h \, dV = 0, \quad (18a)$$

$$\int_{\Omega} \nu^h \left( -\mu^h + \bar{\mu}(c^h) + H(\zeta^h) \right) + \nu_{,A}^h W_A(\zeta^h) \, dV = 0, \quad (18b)$$

$$\int_{\Omega} w_{i,J}^h P_{iJ}(\zeta^h) + w_{i,JK}^h B_{iJK}(\zeta^h) \, dV - \int_{\Gamma^T} w_i^h \bar{T}_i \, dS - \int_{\Gamma^M} Dw_i^h \bar{M}_i \, dS - \int_{\Upsilon^G} w_i^h \bar{G}_i \, dC = 0, \quad (18c)$$

where  $\zeta^h(\mathbf{X}, t)$  is an array of  $c^h$ ,  $c_{,A}^h$ ,  $F_{i,j}^h (= \delta_{ij} + u_{i,j}^h)$ , and  $F_{i,j,k}^h$ , where spatial derivatives are now to be understood in the weak sense.<sup>1</sup>

Note that, setting  $q^h = 1$ ,  $\nu^h = 0$ , and  $\mathbf{w}^h = \mathbf{0}$  in weak formulation (18), one recovers the mass conservation law:

$$\frac{d}{dt} \int_{\Omega} c^h \, dV = 0.$$

On the other hand, assuming that all Dirichlet and Neumann boundary conditions are time-independent and setting  $q^h = \mu^h$ ,  $\nu^h = Dc^h/Dt$ , and  $\mathbf{w}^h = D\mathbf{u}^h/Dt$  in Eqns.(18) and adding them together, one obtains:

$$\frac{d\Pi^h}{dt} = - \int_{\Omega} \mu_{,A}^h L_{AB} \mu_{,B}^h \, dV, \quad (19)$$

where  $\Pi^h$  is the space-discrete total free energy at arbitrary time  $t$  defined as:

$$\Pi^h(t) = \int_{\Omega} \Psi_c(c^h) + \Psi_{s+e}(\zeta^h) \, dV - \int_{\Gamma^T} u_i^h \bar{T}_i \, dS - \int_{\Gamma^M} Du_i^h \bar{M}_i \, dS - \int_{\Upsilon^G} u_i^h \bar{G}_i \, dC, \quad (20)$$

where spatial derivatives should be understood in the weak sense. Recalling that the mobility tensor is positive definite, Eqn.(19) implies non-increasing free energy.

These two properties, mass conservation and non-increasing total free energy, are to be inherited by our space-time discrete formulation developed in Sec.3.2; specifically, the latter furnishes the notion of *stability*.

As is well known, substituting Eqns (13), (11) and (6–8) into (12) leads to a fourth-order PDE in strong form. Its weak counterpart has up to second-order spatial derivatives on the composition, and was the basis for Discontinuous Galerkin-based finite element methods in the work of Wells et al. [11], and more recently for  $C^1$ -continuous IGA-based methods in [8]. Here, we use the split formulation of Eqn (15) because, as shown above, it permits the fields  $c^h$  and  $\mu^h$  to be chosen to lie in the same functional space,  $\mathcal{S}^h$  in the resulting finite dimensional statement of the full problem, Eqn (18). This coincidence of spaces is crucial for satisfaction of the fundamental stability result just derived.

<sup>1</sup>Since  $\mathcal{S}^h \subset C^1(\Omega)$  second spatial derivatives of  $\mathbf{w}^h$  and  $\mathbf{u}^h$  are properly defined only in a weak sense—a technicality that is usually not emphasized in finite dimensional weak forms.

### 3.2 Temporal discretization

We proceed to discretize Eqns.(18) in time to obtain a formulation that produces a solution at time  $t^{n+1}$  given a solution at time  $t^n$ . The proposed time-discrete formulation is given as the following:

Given  $c^{h,n}(\mathbf{X}) \in \mathcal{S}^h$ ,  $\mu^{h,n}(\mathbf{X}) \in \mathcal{S}^h$ ,  $\mathbf{u}^{h,n}(\mathbf{X}) \in \mathcal{V}_u^h$ , seek  $c^{h,n+1}(\mathbf{X}) \in \mathcal{S}^h$ ,  $\mu^{h,n+1}(\mathbf{X}) \in \mathcal{S}^h$ ,  $\mathbf{u}^{h,n+1}(\mathbf{X}) \in \mathcal{V}_u^h$  such that for all  $q^h(\mathbf{X}) \in \mathcal{S}^h$ ,  $\nu^h(\mathbf{X}) \in \mathcal{S}^h$ ,  $\mathbf{w}^h(\mathbf{X}) \in \mathcal{V}_w^h$ :

$$\int_{\Omega} q^h \left\{ \frac{Dc^h}{Dt} \right\}^n + q_{,A}^h \{L_{AB}(c^h)\}^n \{\mu^h\}_{,B}^n dV = 0, \quad (21a)$$

$$\int_{\Omega} \nu^h \left( -\{\mu^h\}^n + \{\bar{\mu}(c^h)\}^n + \{H(\zeta^h)\}^n \right) + \nu_{,A}^h \{W_A(\zeta^h)\}^n dV = 0, \quad (21b)$$

$$\begin{aligned} & \int_{\Omega} w_{i,J}^h \{P_{iJ}(\zeta^h)\}^n + w_{i,JK}^h \{B_{iJK}(\zeta^h)\}^n dV \\ & - \int_{\Gamma^T} w_i^h \{\bar{T}_i\}^n dS - \int_{\Gamma^M} Dw_i^h \{\bar{M}_i\}^n dS - \int_{\Gamma^G} w_i^h \{\bar{G}_i\}^n dC = 0, \end{aligned} \quad (21c)$$

where terms with braces  $\{\cdot\}^n(\mathbf{X})$  represent time-discretizations of those quantities inside the braces  $\cdot(\mathbf{X}, t)$  on the time-interval  $t \in [t^n, t^{n+1}]$ , and they are defined in the rest of this section so that formulation (21) is second-order accurate and unconditionally stable.

Stability analysis presented in Sec.4.2 is greatly motivated by that presented in [5] for the Cahn-Hilliard equation, where  $\{\bar{\mu}(c^h)\}^n$  was defined using dedicated quadrature formulas so that non-increasing chemical free energy would be the direct consequence of the weak formulation. In this work we follow the same course, but, instead of developing special quadrature formulas, we employ the concept of Taylor-series expansion, which enables one to simplify the argument as well as to extend the stability analysis to include the coupling with gradient elasticity.

For convenience we denote by  $\zeta^{h,n}(\mathbf{X})$  the temporal approximation to  $\zeta^h(\mathbf{X}, t^n)$ . In addition we define  $\Delta t := t^{n+1} - t^n$ ,  $\Delta c^h := c^{h,n+1} - c^{h,n}$ ,  $\Delta c_{,A}^h := c_{,A}^{h,n+1} - c_{,A}^{h,n}$ ,  $\Delta F_{iJ}^h := u_{i,J}^{h,n+1} - u_{i,J}^{h,n}$ , and  $\Delta F_{iJ,K}^h := u_{i,JK}^{h,n+1} - u_{i,JK}^{h,n}$ .

We first represent  $\{\bar{\mu}(c^h)\}^n$  in terms of  $c^{h,n}$  and  $c^{h,n+1}$  at each fixed point  $\mathbf{X} \in \Omega$ . To this end we observe that the Taylor-series expansion of  $\Psi_c(c)$  around  $c^{h,n+1}$  leads to the following identity:

$$\begin{aligned} \Psi_c(c^{h,n}) &= \Psi_c(c^{h,n+1}) - \bar{\mu}(c^{h,n+1})\Delta c^h + \frac{1}{2} \frac{d\bar{\mu}}{dc}(c^{h,n+1})(\Delta c^h)^2 - \frac{1}{6} \frac{d^2\bar{\mu}}{dc^2}(c^{h,n+1})(\Delta c^h)^3 + \frac{1}{24} \frac{d^3\bar{\mu}}{dc^3}(\xi)(\Delta c^h)^4 \\ &= \Psi_c(c^{h,n+1}) - \left( \bar{\mu}(c^{h,n+1}) - \frac{1}{2} \frac{d\bar{\mu}}{dc}(c^{h,n+1})\Delta c^h + \frac{1}{6} \frac{d^2\bar{\mu}}{dc^2}(c^{h,n+1})(\Delta c^h)^2 \right) \Delta c^h + \frac{1}{24} \frac{d^3\bar{\mu}}{dc^3}(\xi)(\Delta c^h)^4, \end{aligned} \quad (22)$$

where  $\xi = (1 - \alpha)c^{h,n} + \alpha c^{h,n+1}$  for some  $\alpha$  ( $0 < \alpha < 1$ ) by Taylor's Remainder Theorem at each fixed point  $\mathbf{X}$ . We then define  $\{\bar{\mu}(c^h)\}^n$  as the quantity in the parentheses in (22), that is:

$$\{\bar{\mu}(c^h)\}^n := \bar{\mu}(c^{h,n+1}) - \frac{1}{2} \frac{d\bar{\mu}}{dc}(c^{h,n+1})\Delta c^h + \frac{1}{6} \frac{d^2\bar{\mu}}{dc^2}(c^{h,n+1})(\Delta c^h)^2, \quad (23)$$

so that:

$$\{\bar{\mu}(c^h)\}^n \Delta c^h = \Psi_c(c^{h,n+1}) - \Psi_c(c^{h,n}) + \frac{1}{24} \frac{d^3\bar{\mu}}{dc^3}(\xi)(\Delta c^h)^4, \quad (24)$$

at each fixed point  $\mathbf{X} \in \Omega$ . Identity (24) becomes a convenient tool in the stability analysis encountered in Sec.4, noting that  $d^3\bar{\mu}/dc^3(\xi) > 0$  by definition (3a).

We define  $\{H(\zeta^h)\}^n$ ,  $\{W_A(\zeta^h)\}^n$ ,  $\{P_{iJ}(\zeta^h)\}^n$ , and  $\{B_{iJK}(\zeta^h)\}^n$  in a similar fashion. We first denote by  $\mathcal{D}[\phi; \kappa_c, \kappa_{\nabla c}, \kappa_F, \kappa_{\nabla F}]$  the function obtained by applying operators  $(\partial/\partial c)\Delta c^h$ ,  $(\partial/\partial c_{,A})\Delta c_{,A}^h$ ,  $(\partial/\partial F_{iJ})\Delta F_{iJ}^h$ , and  $(\partial/\partial F_{iJ,K})\Delta F_{iJ,K}^h$  respectively  $\kappa_c$ ,  $\kappa_{\nabla c}$ ,  $\kappa_F$ , and  $\kappa_{\nabla F}$  ( $\kappa_c, \kappa_{\nabla c}, \kappa_F, \kappa_{\nabla F} \geq 0$ ) times to a scalar-valued multi-variate function  $\phi(\zeta)$ . For instance we have:

$$\begin{aligned} \mathcal{D}[\phi; 0, 0, 0, 0] &= \phi, \\ \mathcal{D}[\phi; 1, 0, 2, 1] &= \frac{\partial^4 \phi^n}{\partial c \partial F_{iJ} \partial F_{kL} \partial F_{mN,O}} \Delta c^h \Delta F_{iJ}^h \Delta F_{kL}^h \Delta F_{mN,O}^h = \mathcal{D} \left[ \frac{\partial \phi}{\partial F_{iJ}}; 1, 0, 1, 1 \right] \Delta F_{iJ}^h. \end{aligned}$$

We also define  $\kappa = \kappa_c + \kappa_{\nabla c} + \kappa_F + \kappa_{\nabla F}$ . Taylor-series expansion of  $\Psi_{s+e}(\zeta)$  around  $\zeta^{h,n}(\mathbf{X})$  at a fixed point

$\mathbf{X} \in \Omega$  then leads to the following identity:

$$\begin{aligned}
\Psi_{s+e}(\zeta^{h,n+1}) &= \Psi_{s+e}(\zeta^{h,n}) + \sum_{\kappa \geq 1} \frac{\kappa!}{\kappa_c! \kappa_{\nabla c}! \kappa_F! \kappa_{\nabla F}!} \frac{1}{\kappa!} \mathcal{D}[\Psi_{s+e}; \kappa_c, \kappa_{\nabla c}, \kappa_F, \kappa_{\nabla F}] (\zeta^{h,n}) \\
&= \Psi_{s+e}(\zeta^{h,n}) + \sum_{\substack{\kappa_c \geq 1 \\ \kappa \geq 1}} \frac{\kappa_c}{\kappa} \frac{1}{\kappa_c! \kappa_{\nabla c}! \kappa_F! \kappa_{\nabla F}!} \mathcal{D}[\Psi_{s+e}; \kappa_c, \kappa_{\nabla c}, \kappa_F, \kappa_{\nabla F}] (\zeta^{h,n}) \\
&\quad + \sum_{\substack{\kappa_{\nabla c} \geq 1 \\ \kappa \geq 1}} \frac{\kappa_{\nabla c}}{\kappa} \frac{1}{\kappa_c! \kappa_{\nabla c}! \kappa_F! \kappa_{\nabla F}!} \mathcal{D}[\Psi_{s+e}; \kappa_c, \kappa_{\nabla c}, \kappa_F, \kappa_{\nabla F}] (\zeta^{h,n}) \\
&\quad + \sum_{\substack{\kappa_F \geq 1 \\ \kappa \geq 1}} \frac{\kappa_F}{\kappa} \frac{1}{\kappa_c! \kappa_{\nabla c}! \kappa_F! \kappa_{\nabla F}!} \mathcal{D}[\Psi_{s+e}; \kappa_c, \kappa_{\nabla c}, \kappa_F, \kappa_{\nabla F}] (\zeta^{h,n}) \\
&\quad + \sum_{\substack{\kappa_{\nabla F} \geq 1 \\ \kappa \geq 1}} \frac{\kappa_{\nabla F}}{\kappa} \frac{1}{\kappa_c! \kappa_{\nabla c}! \kappa_F! \kappa_{\nabla F}!} \mathcal{D}[\Psi_{s+e}; \kappa_c, \kappa_{\nabla c}, \kappa_F, \kappa_{\nabla F}] (\zeta^{h,n}) \\
&= \Psi_{s+e}(\zeta^{h,n}) + \left( \sum_{\substack{\kappa_c \geq 1 \\ \kappa \geq 1}} \frac{1}{\kappa} \frac{1}{(\kappa_c - 1)! \kappa_{\nabla c}! \kappa_F! \kappa_{\nabla F}!} \mathcal{D}[H; \kappa_c - 1, \kappa_{\nabla c}, \kappa_F, \kappa_{\nabla F}] (\zeta^{h,n}) \right) \Delta c^h \\
&\quad + \left( \sum_{\substack{\kappa_{\nabla c} \geq 1 \\ \kappa \geq 1}} \frac{1}{\kappa} \frac{1}{\kappa_c! (\kappa_{\nabla c} - 1)! \kappa_F! \kappa_{\nabla F}!} \mathcal{D}[W_A; \kappa_c, \kappa_{\nabla c} - 1, \kappa_F, \kappa_{\nabla F}] (\zeta^{h,n}) \right) \Delta c_{,A}^h \\
&\quad + \left( \sum_{\substack{\kappa_F \geq 1 \\ \kappa \geq 1}} \frac{1}{\kappa} \frac{1}{\kappa_c! \kappa_{\nabla c}! (\kappa_F - 1)! \kappa_{\nabla F}!} \mathcal{D}[P_{iJ}; \kappa_c, \kappa_{\nabla c}, \kappa_F - 1, \kappa_{\nabla F}] (\zeta^{h,n}) \right) \Delta F_{iJ}^h \\
&\quad + \left( \sum_{\substack{\kappa_{\nabla F} \geq 1 \\ \kappa \geq 1}} \frac{1}{\kappa} \frac{1}{\kappa_c! \kappa_{\nabla c}! \kappa_F! (\kappa_{\nabla F} - 1)!} \mathcal{D}[B_{iJK}; \kappa_c, \kappa_{\nabla c}, \kappa_F, \kappa_{\nabla F} - 1] (\zeta^{h,n}) \right) \Delta F_{iJ,K}^h,
\end{aligned} \tag{25}$$

where summations are over all possible combinations of  $\kappa_c$ ,  $\kappa_{\nabla c}$ ,  $\kappa_F$ , and  $\kappa_{\nabla F}$  for each  $\kappa$ . These summations are finite as  $\Psi_{s+e}(\zeta)$  is a multi-variate polynomial function of  $c$ ,  $c_{,A}$ ,  $F_{iJ}$ , and  $F_{iJ,K}$ . Factors in the summation in the first line arise since  $\mathcal{D}[\Psi_{s+e}; \kappa_c, \kappa_{\nabla c}, \kappa_F, \kappa_{\nabla F}] (\zeta^{h,n})$  appears in a straightforward Taylor-series expansion  $\kappa!/\kappa_c! \kappa_{\nabla c}! \kappa_F! \kappa_{\nabla F}!$  times due to this number of possible permutations; for instance, the following terms all reduce to  $(1/3!) \cdot \mathcal{D}[\Psi_{s+e}; 0, 0, 2, 1] (\zeta^{h,n})$  and therefore this term in the above summation is to be multiplied by  $3!/0!0!2!1! = 3$ :

$$\begin{aligned}
&\frac{1}{3!} \frac{\partial^3 \Psi_{s+e}}{\partial F_{iJ} \partial F_{kL} \partial F_{mN,O}} (\zeta^{h,n}) \Delta F_{iJ} \Delta F_{kL} \Delta F_{mN,O}, \\
&\frac{1}{3!} \frac{\partial^3 \Psi_{s+e}}{\partial F_{iJ} \partial F_{mN,O} \partial F_{kL}} (\zeta^{h,n}) \Delta F_{iJ} \Delta F_{mN,O} \Delta F_{kL}, \\
&\frac{1}{3!} \frac{\partial^3 \Psi_{s+e}}{\partial F_{mN,O} \partial F_{iJ} \partial F_{kL}} (\zeta^{h,n}) \Delta F_{mN,O} \Delta F_{iJ} \Delta F_{kL}.
\end{aligned}$$

We then define  $\{H(\zeta^h)\}^n$ ,  $\{W_A(\zeta^h)\}^n$ ,  $\{P_{iJ}(\zeta^h)\}^n$ , and  $\{B_{iJK}(\zeta^h)\}^n$  as those quantities in the parentheses in



(25), or:

$$\begin{aligned} & \{H(\zeta^h)\}^n \\ & := H(\zeta^{h,n}) + \frac{1}{2} \left( \frac{\partial H}{\partial c}(\zeta^{h,n})\Delta c^h + \frac{\partial H}{\partial c,B}(\zeta^{h,n})\Delta c_{,B}^h + \frac{\partial H}{\partial F_{IM}}(\zeta^{h,n})\Delta F_{IM}^h + \frac{\partial H}{\partial F_{IM,N}}(\zeta^{h,n})\Delta F_{IM,N}^h \right) + R^c(\zeta^{h,n}), \end{aligned} \quad (26a)$$

$$\begin{aligned} & \{W_A(\zeta^h)\}^n \\ & := W_A(\zeta^{h,n}) + \frac{1}{2} \left( \frac{\partial W_A}{\partial c}(\zeta^{h,n})\Delta c^h + \frac{\partial W_A}{\partial c,B}(\zeta^{h,n})\Delta c_{,B}^h + \frac{\partial W_A}{\partial F_{IM}}(\zeta^{h,n})\Delta F_{IM}^h + \frac{\partial W_A}{\partial F_{IM,N}}(\zeta^{h,n})\Delta F_{IM,N}^h \right) + R_A^{\nabla c}(\zeta^{h,n}), \end{aligned} \quad (26b)$$

$$\begin{aligned} & \{P_{iJ}(\zeta^h)\}^n \\ & := P_{iJ}(\zeta^{h,n}) + \frac{1}{2} \left( \frac{\partial P_{iJ}}{\partial c}(\zeta^{h,n})\Delta c^h + \frac{\partial P_{iJ}}{\partial c,B}(\zeta^{h,n})\Delta c_{,B}^h + \frac{\partial P_{iJ}}{\partial F_{IM}}(\zeta^{h,n})\Delta F_{IM}^h + \frac{\partial P_{iJ}}{\partial F_{IM,N}}(\zeta^{h,n})\Delta F_{IM,N}^h \right) + R_{iJ}^F(\zeta^{h,n}), \end{aligned} \quad (26c)$$

$$\begin{aligned} & \{B_{iJK}(\zeta^h)\}^n \\ & := B_{iJK}(\zeta^{h,n}) + \frac{1}{2} \left( \frac{\partial B_{iJK}}{\partial c}(\zeta^{h,n})\Delta c^h + \frac{\partial B_{iJK}}{\partial c,B}(\zeta^{h,n})\Delta c_{,B}^h + \frac{\partial B_{iJK}}{\partial F_{IM}}(\zeta^{h,n})\Delta F_{IM}^h + \frac{\partial B_{iJK}}{\partial F_{IM,N}}(\zeta^{h,n})\Delta F_{IM,N}^h \right) + R_{iJK}^{\nabla F}(\zeta^{h,n}), \end{aligned} \quad (26d)$$

where

$$R^c := \sum_{\substack{\kappa_c \geq 1 \\ \kappa \geq 3}} \frac{1}{\kappa (\kappa_c - 1)! \kappa_{\nabla c}! \kappa_F! \kappa_{\nabla F}!} \mathcal{D}[H; \kappa_c - 1, \kappa_{\nabla c}, \kappa_F, \kappa_{\nabla F}], \quad (27a)$$

$$R_A^{\nabla c} := \sum_{\substack{\kappa_{\nabla c} \geq 1 \\ \kappa \geq 3}} \frac{1}{\kappa \kappa_c! (\kappa_{\nabla c} - 1)! \kappa_F! \kappa_{\nabla F}!} \mathcal{D}[W_A; \kappa_c, \kappa_{\nabla c} - 1, \kappa_F, \kappa_{\nabla F}], \quad (27b)$$

$$R_{iJ}^F := \sum_{\substack{\kappa_F \geq 1 \\ \kappa \geq 3}} \frac{1}{\kappa \kappa_c! \kappa_{\nabla c}! (\kappa_F - 1)! \kappa_{\nabla F}!} \mathcal{D}[P_{iJ}; \kappa_c, \kappa_{\nabla c}, \kappa_F - 1, \kappa_{\nabla F}], \quad (27c)$$

$$R_{iJK}^{\nabla F} := \sum_{\substack{\kappa_{\nabla F} \geq 1 \\ \kappa \geq 3}} \frac{1}{\kappa \kappa_c! \kappa_{\nabla c}! \kappa_F! (\kappa_{\nabla F} - 1)!} \mathcal{D}[B_{iJK}; \kappa_c, \kappa_{\nabla c}, \kappa_F, \kappa_{\nabla F} - 1], \quad (27d)$$

so that:

$$\{H(\zeta^h)\}^n \Delta c^h + \{W_A(\zeta^h)\}^n \Delta c_{,A}^h + \{P_{iJ}(\zeta^h)\}^n \Delta F_{iJ}^h + \{B_{iJK}(\zeta^h)\}^n \Delta F_{iJ,K}^h = \Psi_{s+e}(\zeta^{h,n+1}) - \Psi_{s+e}(\zeta^{h,n}), \quad (28)$$

at each fixed point  $\mathbf{X} \in \Omega$ . Finally, other quantities in Eqns.(21) are defined as:

$$\left\{ \frac{Dc^h}{Dt} \right\}^n := \frac{\Delta c^h}{\Delta t}, \quad (29a)$$

$$\{c^h\}^n := [c^{h,n+1} + c^{h,n}]/2, \quad (29b)$$

$$\{\mu^h\}^n := [\mu^{h,n+1} + \mu^{h,n}]/2, \quad (29c)$$

$$\{L_{AB}(c^h)\}^n := [L_{AB}(c^{h,n+1}) + L_{AB}(c^{h,n})]/2, \quad (29d)$$

$$\{\bar{T}_i\}^n := [\bar{T}_i^{n+1} + \bar{T}_i^n]/2, \quad (29e)$$

$$\{\bar{M}_i\}^n := [\bar{M}_i^{n+1} + \bar{M}_i^n]/2, \quad (29f)$$

$$\{\bar{G}_i\}^n := [\bar{G}_i^{n+1} + \bar{G}_i^n]/2, \quad (29g)$$

where  $\bar{T}_i^n(\mathbf{X})$ ,  $\bar{M}_i^n(\mathbf{X})$ , and  $\bar{G}_i^n(\mathbf{X})$  are the components of the boundary tractions at  $t^n$ ,  $\bar{T}_i(\mathbf{X}, t^n)$ ,  $\bar{M}_i(\mathbf{X}, t^n)$ , and  $\bar{G}_i(\mathbf{X}, t^n)$ , respectively.

## 4 Analysis

In this section we prove mass conservation, unconditional stability, and second-order accuracy of the time-integration algorithm proposed in Sec.3.2.

## 4.1 Mass conservation

Provided that Eqns.(21) are satisfied for all  $q^h(\mathbf{X}) \in \mathcal{S}^h$ ,  $\nu^h(\mathbf{X}) \in \mathcal{S}^h$ , and  $\mathbf{w}^h(\mathbf{X}) \in \mathcal{V}_w^h$ , those equations are necessarily satisfied when we substitute the following for these test functions:

$$q^h = 1, \quad \nu^h = 0, \quad \mathbf{w}^h = \mathbf{0}.$$

One then readily obtains:

$$\int_{\Omega} c^{h,n+1} dV = \int_{\Omega} c^{h,n} dV,$$

which implies that mass is conserved from time  $t^n$  to time  $t^{n+1}$ .

## 4.2 Stability

We now investigate stability of the proposed time-integration algorithm. To this end, we assume that all Dirichlet and Neumann boundary conditions are time-independent; that is  $\bar{u}_i$ ,  $\bar{m}_i$ ,  $\bar{g}_i$ ,  $\bar{T}_i$ ,  $\bar{M}_i$ , and  $\bar{G}_i$  are constant in time.

Provided that Eqns.(21) are satisfied for all  $q^h(\mathbf{X}) \in \mathcal{S}^h$ ,  $\nu^h(\mathbf{X}) \in \mathcal{S}^h$ , and  $\mathbf{w}^h(\mathbf{X}) \in \mathcal{V}_w^h$ , those equations are necessarily satisfied when we substitute the following for these test functions:

$$q^h = \{\mu^h\}^n, \quad \nu^h = \left\{ \frac{Dc^h}{Dt} \right\}^n, \quad \mathbf{w}^h = \frac{\mathbf{u}^{h,n+1} - \mathbf{u}^{h,n}}{\Delta t}.$$

We then add the resulting three equations together and use identities (24) and (28) to obtain:

$$\frac{\Pi^{h,n+1} - \Pi^{h,n}}{\Delta t} = - \int_{\Omega} \left( \{\mu^h\}_{,A}^n \{L_{AB}(c^h)\}^n \{\mu^h\}_{,B}^n + \frac{1}{24} \frac{d^3\bar{\mu}}{dc^3}(\xi) \frac{(\Delta c^h)^4}{\Delta t} \right) dV, \quad (30)$$

where  $\Pi^{h,n}$  is the space-time discrete total free energy at  $t = t^n$  defined as:

$$\Pi^{h,n} = \int_{\Omega} \Psi_c(c^{h,n}) + \Psi_{s+e}(\boldsymbol{\zeta}^{h,n}) dV - \int_{\Gamma^T} u_i^{h,n} \bar{T}_i dS - \int_{\Gamma^M} Du_i^{h,n} \bar{M}_i dS - \int_{\Gamma^G} u_i^{h,n} \bar{G}_i dC, \quad (31)$$

where spatial derivatives should be understood in the weak sense. Note that, as the mobility tensor is positive definite and  $d^3\bar{\mu}/dc^3(\xi)$  is positive by definition (3a), the right-hand side of (30) is non-positive. Eqn.(30) therefore states that the discrete total free energy is non-increasing from time  $t^n$  to time  $t^{n+1}$  and the algorithm proposed in Sec.3.2 is necessarily unconditionally stable.

## 4.3 Consistency

We proceed to show second-order accuracy of the proposed scheme. Following the standard treatment for the consistency analysis, we substitute the exact solutions at  $t^n$  and  $t^{n+1}$  to the time-continuous problem (18) for  $c^{h,n}(\mathbf{X})$ ,  $\mu^{h,n}(\mathbf{X})$ ,  $\mathbf{u}^{h,n}(\mathbf{X})$ ,  $c^{h,n+1}(\mathbf{X})$ ,  $\mu^{h,n+1}(\mathbf{X})$ , and  $\mathbf{u}^{h,n+1}(\mathbf{X})$  in the time-discrete formulations (21a), (21b), and (21c); we denote the left-hand sides of the resulting equations by  $I_c^n$ ,  $I_\mu^n$ , and  $I_u^n$ , respectively. The following approximations for an arbitrary function  $\phi(\mathbf{X}, t)$  readily obtained by Taylor-series expansion are of use:

$$\begin{aligned} \frac{\phi(\mathbf{X}, t^{n+1}) + \phi(\mathbf{X}, t^n)}{2} &= \phi(\mathbf{X}, t^n) + \frac{\Delta t}{2} \frac{D\phi}{Dt}(\mathbf{X}, t^n) + O(\Delta t^2), \\ \frac{\phi(\mathbf{X}, t^{n+1}) - \phi(\mathbf{X}, t^n)}{\Delta t} &= \frac{D\phi}{Dt}(\mathbf{X}, t^n) + \frac{\Delta t}{2} \frac{D^2\phi}{Dt^2}(\mathbf{X}, t^n) + O(\Delta t^2), \\ \Delta\phi(\mathbf{X}) &:= \phi(\mathbf{X}, t^{n+1}) - \phi(\mathbf{X}, t^n) = \frac{D\phi}{Dt}(\mathbf{X}, t^n)\Delta t + O(\Delta t^2). \end{aligned}$$

High-order terms  $R^c$ ,  $R_A^{\nabla c}$ ,  $R_{iJ}^F$ , and  $R_{iJK}^{\nabla F}$  defined in (27) being  $O(\Delta t^2)$ , one can for instance show that  $\{P_{iJ}(\boldsymbol{\zeta}^h)\}^n$  given in (26c) can after substitution of the exact solutions be approximated as:

$$\{P_{iJ}(\boldsymbol{\zeta}^h)\}^n = \tilde{P}_{iJ}(\mathbf{X}, t^n) + \frac{\Delta t}{2} \frac{D\tilde{P}_{iJ}}{Dt}(\mathbf{X}, t^n) + O(\Delta t^2),$$

where  $\tilde{P}_{iJ}(\mathbf{X}, t) := P_{iJ}(\boldsymbol{\xi}^h(\mathbf{X}, t))$ . Treating other terms similarly, we can readily show the following:

$$I_c^n = I_c(t^n) + \frac{\Delta t}{2} \frac{dI_c}{dt}(t^n) + O(\Delta t^2), \quad (32a)$$

$$I_\mu^n = I_\mu(t^n) + \frac{\Delta t}{2} \frac{dI_\mu}{dt}(t^n) + O(\Delta t^2), \quad (32b)$$

$$I_u^n = I_u(t^n) + \frac{\Delta t}{2} \frac{dI_u}{dt}(t^n) + O(\Delta t^2), \quad (32c)$$

where  $I_c(t)$ ,  $I_\mu(t)$ , and  $I_u(t)$  are the left-hand sides of Eqns.(18a), (18b), and (18c). Since first two terms of the right-hand side of each equation in (32) are zero, one concludes that the proposed time-integration scheme (21) is of order 2.

We note here that in the above consistency analysis specific formulas for  $R^c$ ,  $R_A^{\nabla c}$ ,  $R_{iJ}^F$ , and  $R_{iJK}^{\nabla F}$  are unimportant. Indeed one can ignore some or all high-order terms existing in  $R^c$ ,  $R_A^{\nabla c}$ ,  $R_{iJ}^F$ , and  $R_{iJK}^{\nabla F}$  when evaluating (26), resulting *reduced formulations* still being second-order accurate. Such reduced formulations are not unconditionally stable any more, but are often equipped with practical accuracy. Requiring less computation, they can work as good alternatives to the original formulation in many problems; see Sec.5.3 for an example.

## 5 Numerical examples

In this section we demonstrate the robustness and accuracy of the numerical formulation proposed in Sec.3. Parameters for the chemical free energy density function  $\Psi_c$  introduced in Eqn.(3a) are set as  $A_1 = 1$  and  $A_2 = 3$  so that this function takes its maximum at  $c = 0.5000$  and minimum around  $c = 0.0707$  and  $0.9293$ . Fig.1 shows plots of  $\Psi_c$  against chemical concentration  $c$ , where the chemical spinodal region is also shown as the interval between two dashed lines. We denote by  $d(= 0.1152)$  the difference between the maximum and minimum values of  $\Psi_c$ . The diffusion and mobility tensors appearing in Eqn.(3b) and in Eqn.(12), respectively, are defined as  $K_{AB}(c) = 2^{-6}\delta_{AB}$  and  $L_{AB}(c) = 6c(1-c)\delta_{AB}$ . Parameters for the mechanical free energy density function  $\Psi_e$  defined in Eqn.(3c) are given as  $e_{\text{chem}} = -1/16 \cdot (c - 0.48)$ ,  $B_1(c) = 13/4 \cdot \mu$ ,  $B_2(c) = -5/32 \cdot \mu(c - 0.50)$ ,  $B_3(c) = 1/4 \cdot \mu(c - 0.50)$ ,  $B_4(c) = \mu$ ,  $B_5(c) = 2\mu$ , and  $B_6(c) = 2^{-14}\mu c$ , where  $\mu = 2^{11}d$ .  $\Psi_e$  thus defined characterizes crystallographic structural changes between a cubic phase and three symmetric tetragonal phases; cubic phase loses stability and transforms into one of three stable tetragonal phases as the local concentration  $c$  increases. This transformation is represented by the projection of  $\Psi_e$  onto the  $e_2 - e_3$  plane, which experiences a continuous transition from convex to non-convex functions with respect to  $e_2$  and  $e_3$ , exhibiting *three-wells* on the  $e_2 - e_3$  plane for  $c > 0.5$ ; see Figs.2. The distance on the  $e_2 - e_3$  plane from the origin to these three minima is designed to be  $1/4$  when  $c = 1$ ; that is, minima occur at  $(+\sqrt{3}/8, +1/8)$ ,  $(-\sqrt{3}/8, +1/8)$ , and  $(0, -1/4)$ , each corresponding to a rectangular crystal structure that is elongated in the  $X$ -,  $Y$ -, or  $Z$ - direction, respectively. Stable crystal structures are also depicted in Figs.2. We also note here that, to compute  $\{H(\zeta^h)\}^n$ ,  $\{W_A(\zeta^h)\}^n$ ,  $\{P_{iJ}(\zeta^h)\}^n$ , and  $\{B_{iJK}(\zeta^h)\}^n$  defined in (26) and (27), one needs to take derivatives of  $\Psi_{s+e}(\zeta)$  with respect to  $c$ ,  $c_A$ ,  $F_{iJ}$ , and  $F_{iJK}$ , respectively, 2, 2, 8, and 2 times; it is therefore sufficient to set  $\kappa_c \leq 2$ ,  $\kappa_{\nabla c} \leq 2$ ,  $\kappa_F \leq 8$ , and  $\kappa_{\nabla F} \leq 2$ .

The reference domain occupies a unit cube  $\mathbf{X} \in \Omega = (0, 1)^3$  and we set boundary conditions as  $u_i = 0$  and  $Du_i = 0$  on  $Z = 0$ ,  $\bar{T}_i = 0$  and  $\bar{M}_i = 0$  on  $Z = 1$ , and  $u_k N_k = 0$ ,  $\bar{T}_i - \bar{T}_k N_k N_i = 0$ , and  $\bar{M}_i = 0$  on  $X, Y = 0, 1$ . Further, we set  $G_i = 0$  on all edges where  $u_i = 0$  is not specified.

We employ IGA to numerically solve our example problems, where three-dimensional basis is comprised of tensor product of one-dimensional second-order B-spline basis on uniformly spaced *knots*.

The initial condition of the local concentration  $c$  is produced on a coarse  $2^3$  mesh that has 2 *elements*, or 4 basis functions, in each direction. The primitive one-dimensional B-spline basis functions in  $X$ -,  $Y$ -, and  $Z$ -directions are indexed as  $i_X$ ,  $i_Y$ , and  $i_Z$ , where  $i_X, i_Y, i_Z = 0, 1, 2, 3$ , and *control points* for  $i_X, i_Y, i_Z = 1, 2$  are given as  $0.48 + 0.01 \sin(999 \sin(997i_X + 991i_Y + 983i_Z + 1))$  and those for  $i_X, i_Y, i_Z = 0, 3$  are computed to satisfy the boundary condition (10b). This initial condition is projected onto finer meshes ( $16^3$ ,  $32^3$ , and  $64^3$

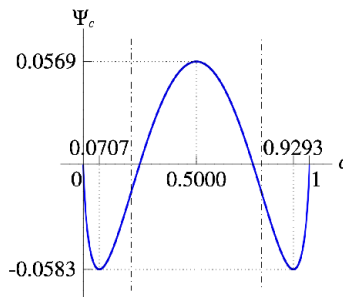


Figure 1: Plots of chemical free energy density function  $\Psi_c$  against chemical concentration  $c$  for parameters used in our example problems.

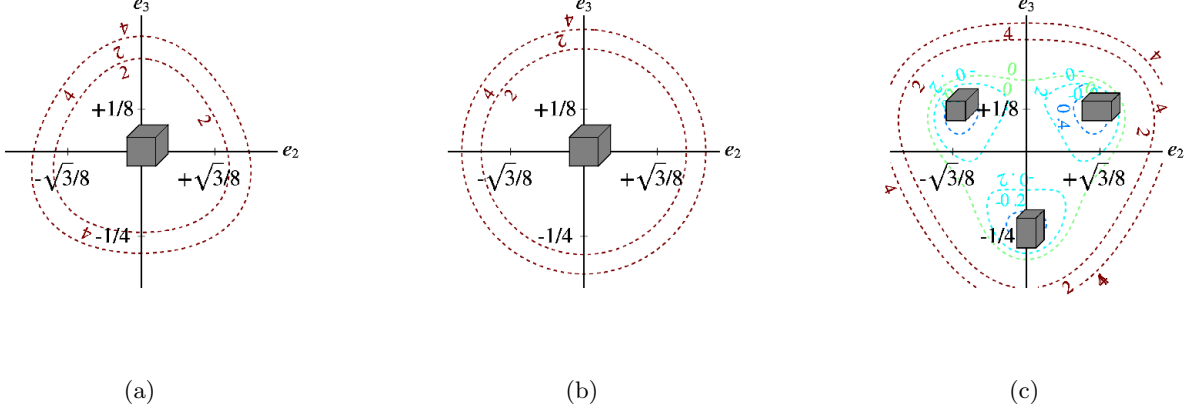


Figure 2: Contour plots of the projection of the mechanical free energy density function  $\Psi_e$  onto the  $e_2 - e_3$  plane for (a)  $c = 0.0707$ , (b)  $c = 0.5000$ , and (c)  $c = 0.9293$ . Corresponding stable crystal structures are also depicted.

meshes) *exactly* by successive uniform  $h$ -refinements by *knot-insertions* [3]. Finally, initial conditions for the chemical potential and the displacement field are given as  $\mu = 0$  and  $u_i = 0$ .

We solve all problems using our primitive software specifically designed for the unconditionally stable time-integration algorithm proposed in Sec.3 for three-dimensional mechano-chemical problems, which uses PETSc 3.5 for linear/nonlinear solvers and `mathgl` 2.3 for plotting. We also utilized `Mathematica` 10 to compute high-order indicial sums appearing in (26) and (27) as well as to compute tangent matrices required for nonlinear solvers.

## 5.1 Temporal accuracy

In this section we study temporal accuracy of our proposed formulation consistently using a  $32^3$  mesh. We use various timesteps  $\Delta t = 4 \cdot 10^{-3}$ ,  $2 \cdot 10^{-3}$ ,  $1 \cdot 10^{-3}$ ,  $5 \cdot 10^{-4}$ , and  $2.5 \cdot 10^{-4}$  and time-integrate up to  $t = 4$  at which solutions are regarded as sufficiently stationary.

Fig.3 shows color plots of  $e_2$  along with contour curves of  $c$  for solutions obtained using  $\Delta t = 4 \cdot 10^{-3}$ ,  $2 \cdot 10^{-3}$ ,  $1 \cdot 10^{-3}$ , and  $5 \cdot 10^{-4}$ . While  $\Delta t = 4 \cdot 10^{-3}$  leads to a completely different morphological evolution implying insufficient temporal resolution, absence of visible change in solutions for  $\Delta t = 2 \cdot 10^{-3}$ ,  $1 \cdot 10^{-3}$ , and  $5 \cdot 10^{-4}$  indicates convergence of the microstructure as timesteps are refined.

Figs.4a and 4b show plots of discrete total free energy  $\Pi^{h,n}$  against time for  $t \in [0, 4]$  and  $t \in [0.9, 1.1]$ , respectively, for solutions corresponding to  $\Delta t = 4 \cdot 10^{-3}$ ,  $2 \cdot 10^{-3}$ ,  $1 \cdot 10^{-3}$ , and  $5 \cdot 10^{-4}$ , where one can also observe energetical convergence of the solutions with timestep refinement. We also note that the discrete free energy is non-increasing for any timesteps, implying unconditional stability of our proposed time-discrete formulation as expected from the analysis in Sec.4.2.

Finally, we regard the solution for  $\Delta t = 2.5 \cdot 10^{-4}$  as exact and compute the discrete free energy error  $e = \Psi^{h,n+1} - \Psi^{h,n}$  at  $t = 1$  for each solution. Fig.4c shows plots of absolute error  $|e|$  at  $t = 1$  against timestep  $\Delta t$  in log-log scale, where one observes a second-order temporal convergence as expected from the analysis in Sec.4.3.

## 5.2 Spatial convergence

We continue in this section to investigate spatial convergence of the solutions with mesh refinement. We solve problems on three different meshes,  $16^3$ ,  $32^3$ , and  $64^3$ , using a fixed timestep  $\Delta t = 2 \cdot 10^{-3}$  that is regarded as small enough. Time-integration is again performed up to  $t = 4$ . Fig.5 shows temporal evolution of microstructure on these three meshes. One observes that, while  $16^3$  mesh seems under-resolved, no further morphological changes appear under refinement from  $32^3$  mesh to  $64^3$  mesh, which gives a good evidence of spatial convergence of the microstructure. Solution on  $64^3$  mesh with  $\Delta t = 1 \cdot 10^{-3}$  is also plotted to show that  $\Delta t = 2 \cdot 10^{-3}$  gives sufficient temporal resolution for this spatial convergence analysis. Figs.6a and 6b show plots of corresponding discrete total free energy  $\Pi^{h,n}$  against time for  $t \in [0, 4]$  and  $t \in [0.9, 1.1]$ , respectively, where one can further observe energetical convergence of the solutions under mesh refinement. Discrete total free energy plots for the solution on  $64^3$  mesh with  $\Delta t = 1 \cdot 10^{-3}$  are also shown, which further assures that timestep of  $\Delta t = 2 \cdot 10^{-3}$  is small enough for this observation.

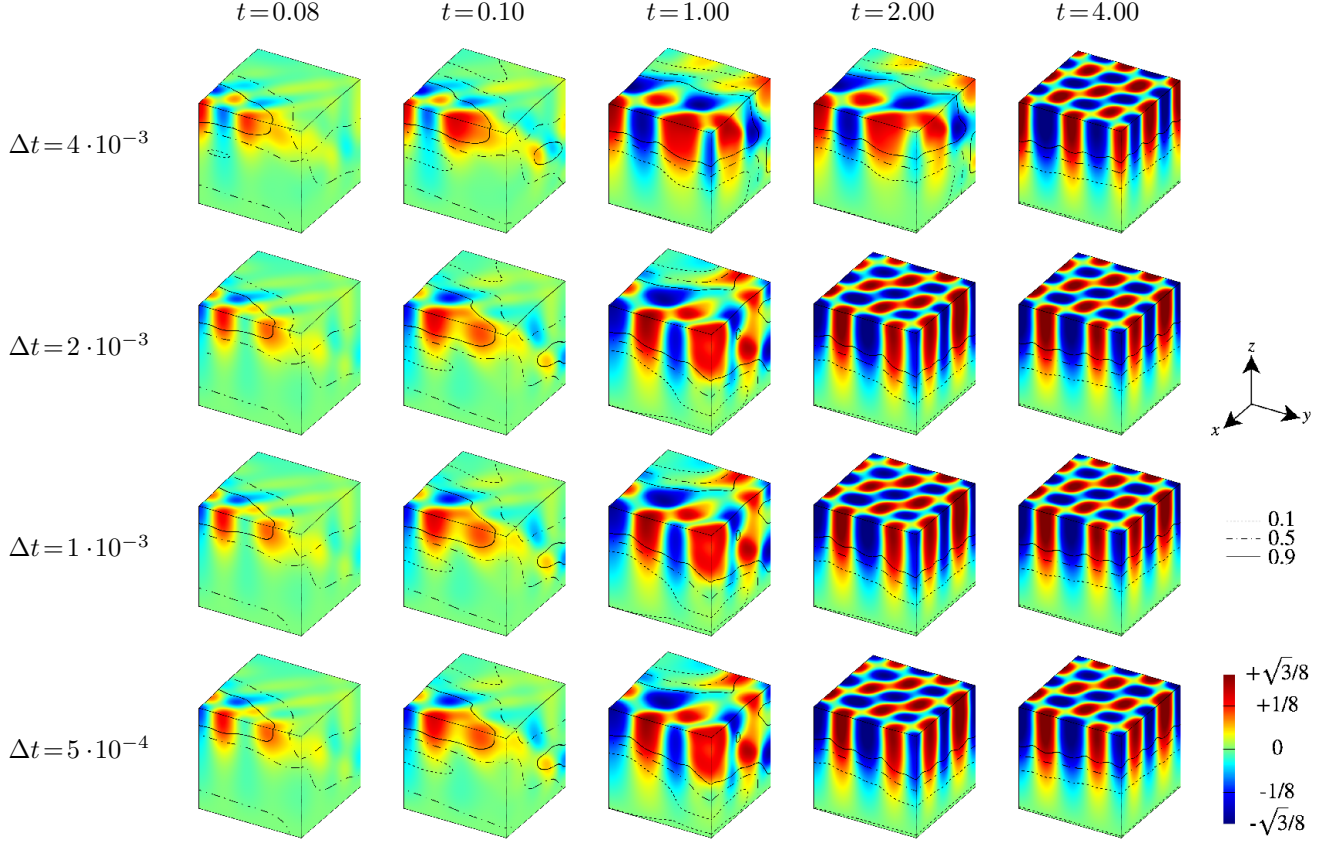


Figure 3: Color plots of  $e_2$  and contour curves of  $c$  on deformed configurations at select time for solutions corresponding to four different timesteps  $\Delta t = 4 \cdot 10^{-3}$ ,  $2 \cdot 10^{-3}$ ,  $1 \cdot 10^{-3}$ , and  $5 \cdot 10^{-4}$  on a  $32^3$  mesh.

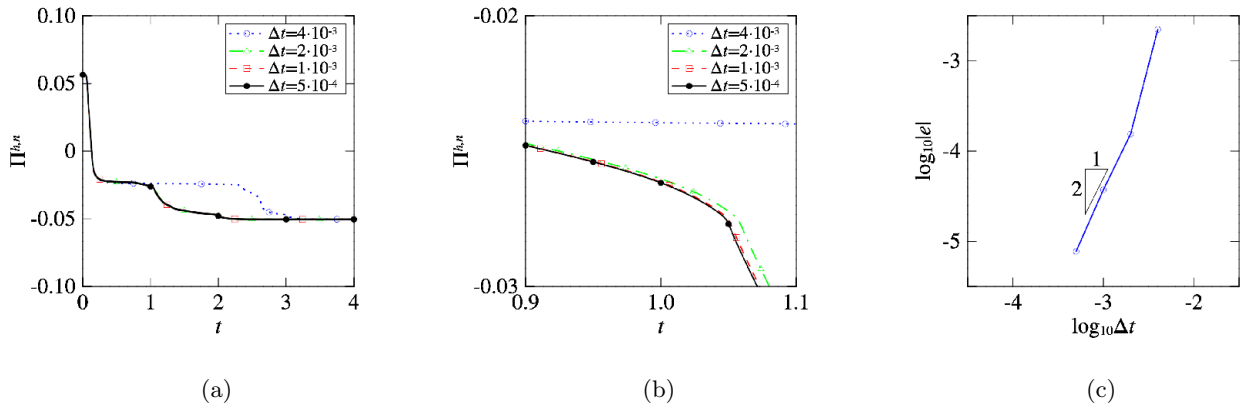


Figure 4: Plots of discrete total free energy  $\Pi^{h,n}$  against time  $t$  for (a)  $t \in [0, 4]$  and (b)  $t \in [0.9, 1.1]$  for four different timesteps  $\Delta t = 4 \cdot 10^{-3}$ ,  $2 \cdot 10^{-3}$ ,  $1 \cdot 10^{-3}$ , and  $5 \cdot 10^{-4}$ . (c) Plots of discrete total free energy error  $|e|$  at  $t = 1$  against timestep  $\Delta t$  in log-log scale. A fixed  $32^3$  mesh was used.

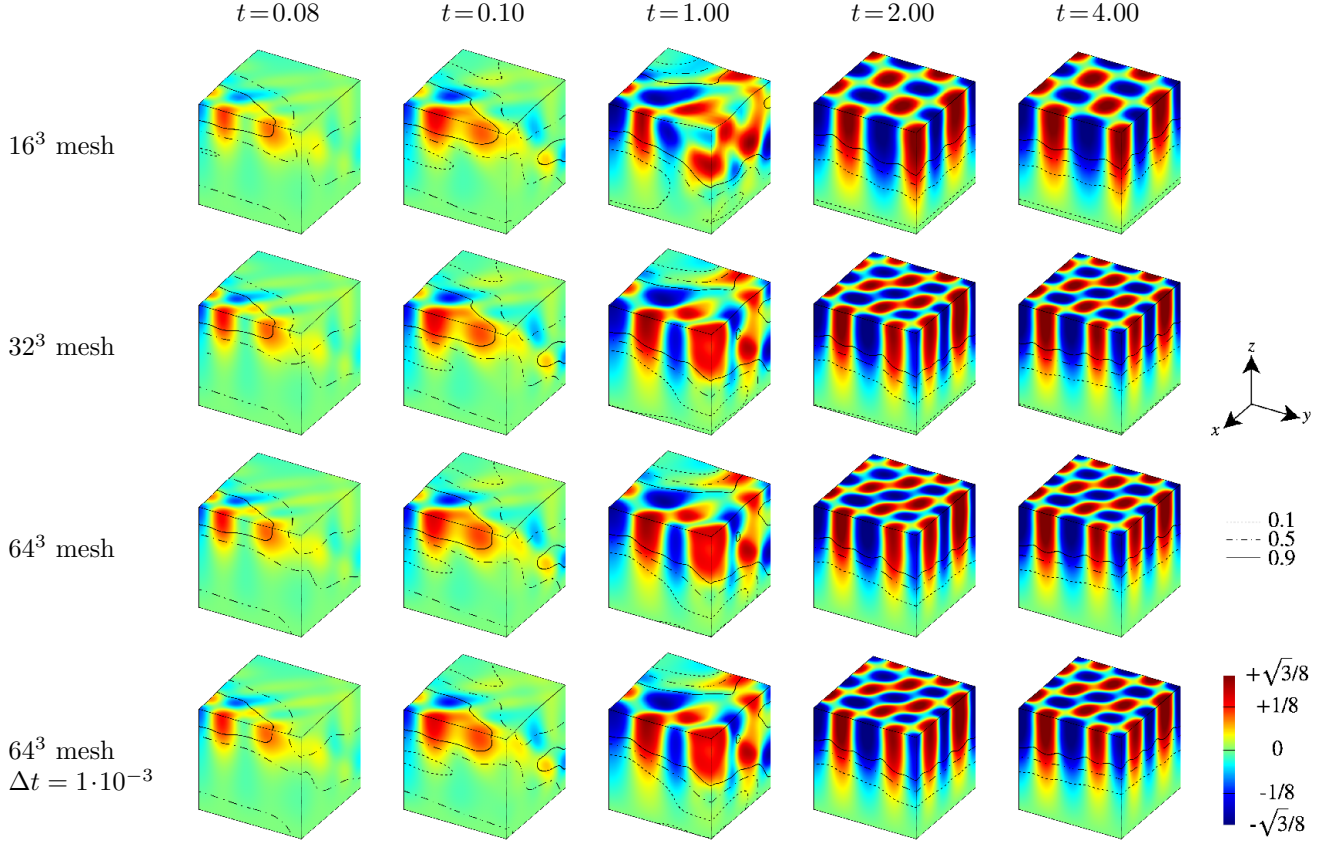


Figure 5: Color plots of  $e_2$  and contour curves of  $c$  on deformed configurations at select time for solutions computed on three different meshes,  $16^3$ ,  $32^3$  and  $64^3$  with  $\Delta t = 2 \cdot 10^{-3}$ . Solution on a  $64^3$  mesh with  $\Delta t = 1 \cdot 10^{-3}$  is also shown for comparison.

We conclude this section by investigating the converged microstructure obtained in our numerical analysis. Figs.7a and 7b show the top views of color plots of  $e_2$  and  $e_3$  in current configuration at  $t = 4$  computed on  $64^3$  mesh with  $\Delta t = 2 \cdot 10^{-3}$ . These top views are overlaid with distorted  $32^2$  meshes for a better visualization of the deformation, with which one observes twin boundaries between two of the three tetragonal variants, viz. those two living in the upper-half plane in Fig.2c. Figs.7a and 7b also show the ability of the proposed formulation to deal with large deformation. Fig.7c shows dot plots of  $(e_2, e_3)$  computed at uniformly spaced  $64^2$  points on  $Z = 1$  along with the contour plots shown in Fig.2c. Distribution of values of  $(e_2, e_3)$  is reasonable considering the strong constraint by the boundaries and relatively large chemical diffusivity that we use in this example.

### 5.3 Reduced formulations

We have so far evaluated  $\{\bar{\mu}(c^h)\}^n$ ,  $\{H(\zeta^h)\}^n$ ,  $\{W_A(\zeta^h)\}^n$ ,  $\{P_{iJ}(\zeta^h)\}^n$ , and  $\{B_{iJK}(\zeta^h)\}^n$  exactly in (26) according to (27), setting  $\kappa_c \leq 2$ ,  $\kappa_{\nabla c} \leq 2$ ,  $\kappa_F \leq 8$ , and  $\kappa_{\nabla F} \leq 2$ . In this section we introduce a reduced formulation in which some high-order terms in  $\{\bar{\mu}(c^h)\}^n$ ,  $\{H(\zeta^h)\}^n$ ,  $\{W_A(\zeta^h)\}^n$ ,  $\{P_{iJ}(\zeta^h)\}^n$ , and  $\{B_{iJK}(\zeta^h)\}^n$  are ignored; specifically, we consider the formulation obtained by setting  $\kappa_F \leq 4$  instead of  $\kappa_F \leq 8$ . This reduced formulation is *not* unconditionally stable, but often provides solutions of sufficient quality at smaller computational costs.

To demonstrate this point we solve the example problem encountered in Sec.5.1 on a  $32^3$  mesh with  $\Delta t = 5 \cdot 10^{-4}$  up to  $t = 4$  using this reduced formulation and compare the solution with that obtained by using the exact formulation.

Using 2.60GHz Intel Xeon E5-2670 processors on  $8 \times 8 \times 8$  partitions, actual time required for the time-integration was measured for each formulation. The results are summarized in Table 1, where one observes 30% reduction of the computational time in the reduced formulation.

Fig.8 shows color plots of  $e_2$  and contour curves of  $c$  for these solutions at select time  $t$  and Fig.9a and 9b show plots of corresponding discrete total free energy  $\Pi^{h,n}$  against time for  $t \in [0, 4]$  and  $t \in [0.9, 1.1]$ , respectively. In these figures two solutions obtained by the reduced formulation corresponding  $\kappa_F \leq 4$  and

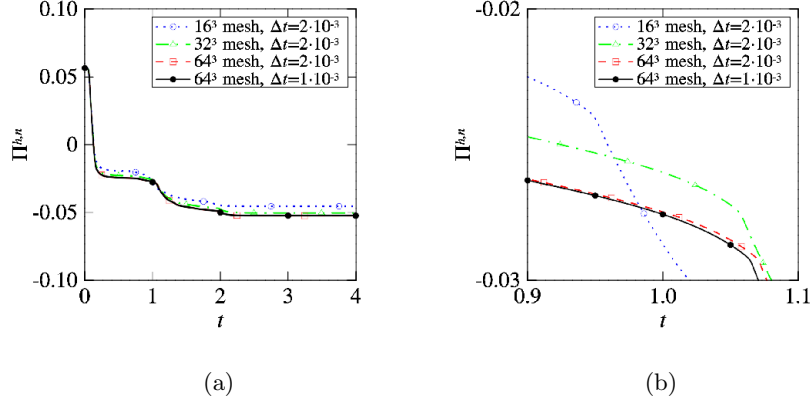


Figure 6: Plots of discrete total free energy  $\Pi^{h,n}$  against time  $t$  for (a)  $t \in [0, 4]$  and (b)  $t \in [0.9, 1.1]$  for three different meshes,  $16^3$ ,  $32^3$ , and  $64^3$ , with timestep  $\Delta t = 2 \cdot 10^{-3}$ . Solution on  $64^3$  mesh with  $\Delta t = 1 \cdot 10^{-3}$  is also shown for comparison.

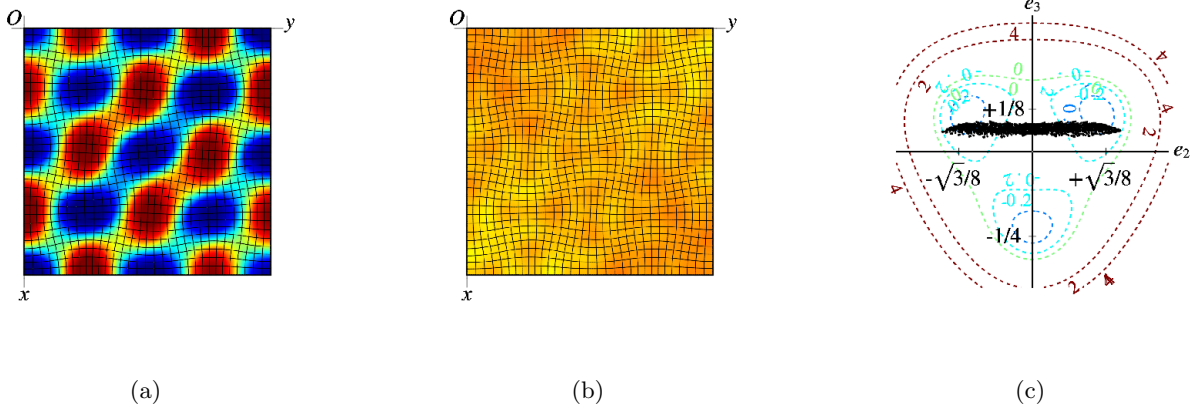


Figure 7: Top views of color plots of (a)  $e_2$  and (b)  $e_3$  on  $Z = 1$  obtained on the  $64^3$  mesh with  $\Delta t = 2 \cdot 10^{-3}$ , which are overlaid with  $32^2$  plotting meshes. (c) Dot plots of  $e_2$  and  $e_3$  values computed on  $Z = 1$  at uniformly spaced  $64^2$  points over the contour plots shown in Fig.2c.

formulation	computation time [hours]
$\kappa_F \leq 4$	64
$\kappa_F \leq 8$	93

Table 1: Time required to compute solutions up to  $t = 4$  on  $32^3$  mesh with  $\Delta t = 5 \cdot 10^{-4}$  using 2.60GHz Intel Xeon E5-2670 processors on  $8 \times 8 \times 8$  partitions for a reduced formulation and the full formulation corresponding to  $\kappa_F \leq 4$  and  $\kappa_F \leq 8$ , respectively.

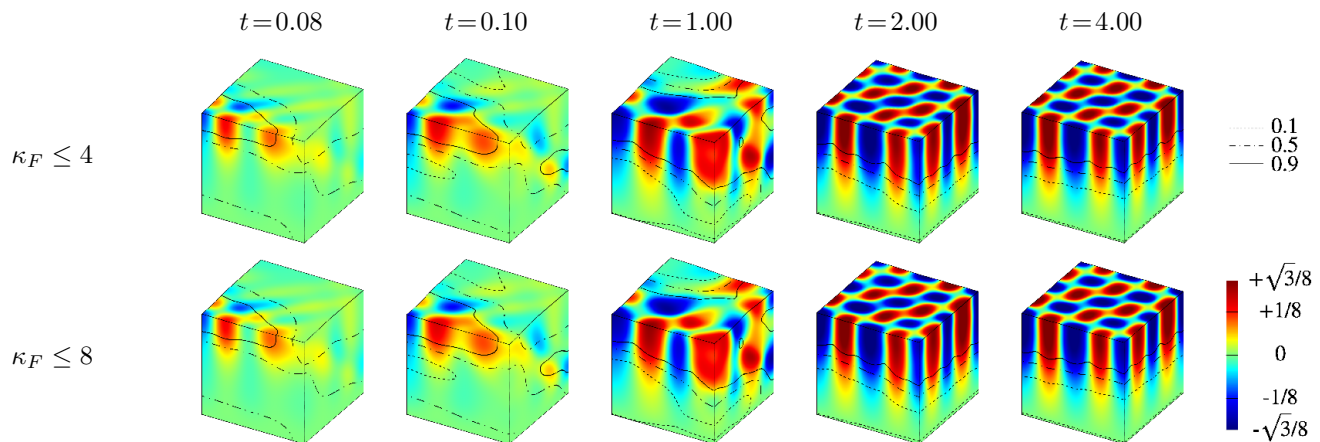


Figure 8: Color plots of  $e_2$  and contour curves of  $c$  on deformed configurations at select time for two formulations corresponding to  $\kappa_F \leq 4$  and  $\kappa_F \leq 8$ . Solutions were computed on a  $32^3$  mesh with  $\Delta t = 5 \cdot 10^{-4}$ .

the full formulation corresponding to  $\kappa_F \leq 8$  are indistinguishable, indicating that, despite the possible loss of unconditional stability, the reduced formulation can produce solutions that are of sufficient quality in practice and can serve as an alternative to the full formulation when faster time-integration is demanded.

## 6 Conclusion

We have developed a class of unconditionally stable, second-order accurate time-integration algorithms for a class of nonlinear, mechano-chemical problems characterized by free energy functions that are non-convex in strain-composition space, and that must be stabilized by introducing spatial gradients of these fields. The associated phenomenology, which we term as mechano-chemical spinodal decomposition, includes the formation of microstructural features and transient phenomena. Their resolution by first-order schemes such as the Backward Euler algorithm does not necessarily preserve the free energy decay that is a consequence of the second law of thermodynamics.

The approach presented here has wide applicability to design stable, second-order schemes for coupled problems of mechanics and transport. Its use hinging on the Taylor-series expansion, can, in principle, be extended to any free energy function that is of polynomial form. Such functions are guaranteed to have finite Taylor-series expansions, and therefore, analytic formulas for the constitutive relations. We note that our approach, although motivated by that of Gómez & Hughes [5], is fundamentally different in that those authors employed special quadrature formulas to ensure stability of their formulation. While evaluation of the Taylor series expansions in the code comes at a cost, we have found that by exploiting symmetries inherent in the higher-order derivatives this cost can be substantially reduced. Furthermore, we have demonstrated that reduced formulations that truncate the higher-order terms in the Taylor series also perform well for the initial and boundary value problems we have considered, maintaining stability, even though unconditional stability can no longer be proven. *Our analysis demonstrates, however, that second-order accuracy is maintained, regardless.*

To the best of our knowledge, this is the first treatment presenting stable and second-order schemes for systems that incorporate Toupin's theory of gradient elasticity at finite strains. It has potential for extension to problems incorporating advection and reaction terms in the transport equation, as well as to systems that couple with the Allen-Cahn [1] treatment for evolution of non-conserved order parameters. It could thus cover a wide range of phase transformation phenomena involving solids as well as fluid phases in materials systems arising in battery, semi-conductor, polymer and structural applications.



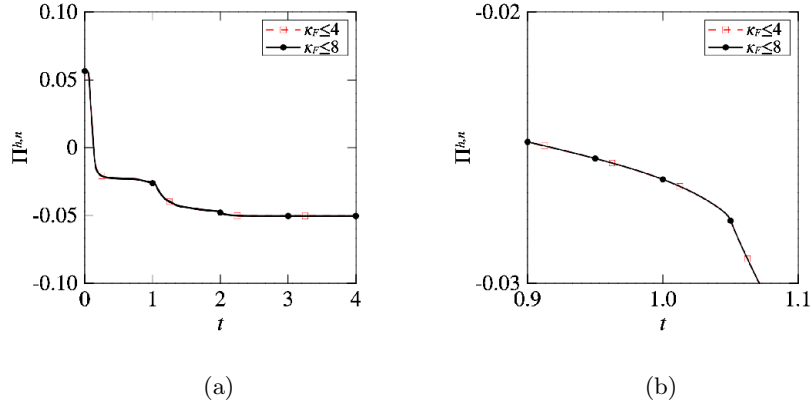


Figure 9: Plots of discrete total free energy  $\Pi^{h,n}$  against time  $t$  for (a)  $t \in [0, 4]$  and (b)  $t \in [0.9, 1.1]$  for two formulations corresponding to  $\kappa_F \leq 4$  and  $\kappa_F \leq 8$ . Solutions were computed on a  $32^3$  mesh with  $\Delta t = 5 \cdot 10^{-4}$ .

## References

- [1] S.M. Allen and J.W. Cahn, *A microscopic theory for antiphase boundary motion and its application to antiphase boundary coarsening*, Acta Metallurgica **27** (1979), 1085–1091.
- [2] J.W. Cahn and J.E. Hilliard, *Free energy of a nonuniform system. I. interfacial energy*, Journal of Chemical Physics **28** (1958), 258–267.
- [3] J. Austin Cottrell, Thomas J. R. Hughes, and Yuri Bazilevs, *Isogeometric Analysis*, John Wiley & Sons, Ltd, 2009.
- [4] Héctor Gómez, Victor M. Calo, Yuri Bazilevs, and Thomas J.R. Hughes, *Isogeometric analysis of the Cahn-Hilliard phase-field model*, Computer Methods in Applied Mechanics and Engineering **197** (2008), no. 49-50, 4333 – 4352.
- [5] Héctor Gómez and Thomas J.R. Hughes, *Provably unconditionally stable, second-order time-accurate, mixed variational methods for phase-field models*, Journal of Computational Physics **230** (2011), no. 13, 5310 – 5327.
- [6] Daozhi Han and Xiaoming Wang, *A second order in time, uniquely solvable, unconditionally stable numerical scheme for Cahn-Hilliard-Navier-Stokes equation*, Journal of Computational Physics **290** (2015), no. 0, 139 – 156.
- [7] S. Rudraraju, A. Van der Ven, and K. Garikipati, *Three-dimensional isogeometric solutions to general boundary value problems of Toupin’s gradient elasticity theory at finite strains*, Computer Methods in Applied Mechanics and Engineering **278** (2014), 705 – 728.
- [8] S. Rudraraju, A. Van der Ven, and K. Garikipati, *Mechano-chemical spinodal decomposition: A phenomenological theory of phase transformations in multi-component crystalline solids*, in review, 2015.
- [9] R.A. Toupin, *Theories of elasticity with couple-stress*, Archive for Rational Mechanics and Analysis **17** (1964), no. 2, 85–112.
- [10] P. Vignal, L. Dalcin, D. L. Brown, N. Collier, and V. M. Calo, *An energy-stable convex splitting for the phase-field crystal equation*, arXiv:1405.3488 (2014).
- [11] G.N. Wells, E. Kuhl, and K. Garikipati, *A Discontinuous Galerkin method for the Cahn-Hilliard equation*, Journal of Computational Physics **218** (2006), 860 – 877.